Rare Met. (2018) 37(2):123–128
https://doi.org/10.1007/s12598-017-0937-2

RARE METALS
www.editorialmanager.com/rmet

Controlled pore size of Pt/KIT-6 used for propane total oxidation

Yu-Sheng Chen, Yi-Dan Cao, Rui Ran*, Xiao-Dong Wu, Duan Weng

Received: 29 July 2016 / Revised: 13 September 2016 / Accepted: 23 May 2017 / Published online: 7 July 2017

Abstract Mesoporous silica KIT-6 with different pore sizes was controllably synthesized by hydrothermal methods. The same contents of Pt were loaded on KIT-6 supports to apply for propane total oxidation. Low-angle X-ray diffraction (XRD), nitrogen adsorption–desorption, CO chemisorption and transmission electron microscopy (TEM) were carried out to investigate the physicochemical properties of the catalysts. The results reveal that different pore sizes of KIT-6 supports could affect the Pt particle sizes on KIT-6. The mesopores on KIT-6-80 and KIT-6-130 effectively confine the size of the inside Pt nanoparticles during calcining. Pt/KIT-6-80 with the appropriate pore size as well as the Pt particle size exhibits the best catalytic performance with T_{50} (the temperature at which hydrocarbon (HC) conversion reaches 50%) of only 237 °C. However, Pt particles prefer dispersing on the external surface of KIT-6-40 due to those too small pores.

Keywords Mesoporous silica; KIT-6; Pore size; Propane total oxidation

Y.-S. Chen, Y.-D. Cao, R. Ran*, X.-D. Wu
Key Laboratory of Advanced Materials of Ministry of Education, School of Materials Science and Engineering, Tsinghua University, Beijing 100084, China
e-mail: ranr@tsinghua.edu.cn

X.-D. Wu, D. Weng
State Key Laboratory of New Ceramics and Fine Processing, School of Materials Science and Engineering, Tsinghua University, Beijing 100084, China

1 Introduction

The trend in modern vehicular diesel engines has been towards the lower compression ratios to improve power density and reduce emissions [1]. Cold-start technology becomes a mainstream technology in diesel engines development. Owing to slow warm-up rates on cold-start diesel engines, significant time is required for the exhaust to reach 200 °C [2]. Exhaust gases therefore contain large amounts of unburned hydrocarbons during the cold starting period. To reduce these cold-start hydrocarbon (HC) emissions, diesel oxidation catalysts (DOCs) with both high activities and low operating temperatures would be desirable. In spite of their expensive costs, Pt supported on high-surface-area supports is the most widely used in current commercial DOCs because of their high specific activity, resistance to deactivation and ability to be regenerated [3–5].

Pt/Al_2O_3 is one of the typical DOCs applied in current commercial oxidation catalysts installed in diesel-driven vehicles [6]. However, the efficient oxidation of saturated hydrocarbons on Pt/Al_2O_3 catalyst generally requires relative high temperatures. T_{50} (the temperature at which HC conversion reaches 50%) of the light-off curves over Pt/Al_2O_3 was generally as high as 350 °C [7–9]. Supports and additives had great effects on the oxidative activity of Pt catalysts. Yoshida et al. [7] reported that the Pt catalysts on the more acidic support showed higher activity, and the catalytic activity on each of the chosen support materials increased as the electronegativity of additives increased. Avila et al. [9] used CeO_2 and TiO_2 as the replacements of Al_2O_3. It was found that the propane oxidation turnover rates of Pt/CeO_2 and Pt/TiO_2 were much higher than that of Pt/Al_2O_3. T_{50} of the light-off curves over Pt/CeO_2 and Pt/TiO_2 could be 60 °C lower than that of Pt/Al_2O_3.

With the combination of uniform pore sizes, ultra-high surface area and good stability under high-temperature environment, zeolites [10–12] are considered as ideal support materials in advanced catalysts design. Garetto et al. [13] applied several commercial zeolites to support Pt catalyst, and the obtained activities on low-carbon alkane oxidation were enhanced. The light-off temperatures of three alkanes were 50–150 °C lower than that of Al_2O_3, respectively. Boulaoued et al. [14] loaded Mo and Fe with different ratios on mesoporous silica KIT-6 and used them for methylcyclopentane total conversion. And they found that the highly dispersed FeO_x nanoclusters in KIT-6 were responsible for rupturing the endocyclic C–C bonding. Liu et al. [15] prepared SBA-15-supporting Ni catalysts and found that Ni/SBA-15 showed higher catalytic activity on ammonia decomposition than other typical Ni-based catalysts and even Ru-based catalysts. Anpo et al. [16] reported that the zeolite structure with larger pore sizes and 3D channel in MCM-41 and MCM-48 can not only help metal ions highly disperse but also achieve high photocatalytic efficiency on reduction reaction of CO_2 and H_2O.

In previous work, it was found that Pt in mesoporous SBA-15 and KIT-6 exhibited superior catalytic activities for propane total oxidation in comparison to the conventional Pt/Al_2O_3 catalyst [8]. And the Pt nanoparticles in KIT-6 were even smaller with homogeneous size distribution and existed in lower oxidation states, which were beneficial to the catalytic activity. To continue the deep investigation on the effects of pore size of KIT-6 on Pt dispersion as well as the oxidative catalytic activity, in this paper, three KIT-6 samples with different pore sizes were controllably synthesized. 1 wt% Pt was loaded on each of the KIT-6 supports to apply for total oxidation of propane. The physicochemical properties of the prepared catalysts were investigated. The enforced ageing on such catalysts was also carried out to investigate their resistance to high-temperature conditions.

2 Experimental

The support materials KIT-6 were obtained according to the procedure reported by Soni et al. [17] using a triblock copolymer (P123, Sigma-Aldrich) as the structure-directing agent. During the synthesis, 6 g P123 was dissolved in 200 g distilled water and 10 g concentrated HCl (35 vol%). After P123 completely dissolved in the solution, 6 g 1-butanol was added with stirring at 35 °C for 1 h. Then 12.9 g tetraethyl orthosilicate (TEOS) was added dropwise and the mixed solution was stirred under 35 °C for 24 h, and then it was transferred to Teflon container and hydrothermal treatment was applied in a close condition for 24 h at 40, 80 and 130 °C, respectively. The obtained solid products were separated by filter and dried for 24 h under 80 °C. Calcining was carried out at 550 °C for 6 h to burn the remaining templates. The as-received powders were denoted as KIT-6-40, KIT-6-80 and KIT-6-130, respectively. The supported Pt catalysts were prepared by incipient wetness method using the platinum nitrate as the precursor. The metal loading ratio of Pt on KIT-6 was 1 wt%. Each catalyst was dried at 100 °C for 12 h after impregnation and then calcined at 500 °C for 3 h. The supported Pt catalysts were denoted as Pt/KIT-6-40, Pt/KIT-6-80 and Pt/KIT-6-130, respectively. The high-temperature ageing condition was 800 °C continuous calcining for 12 h in flowing air with 10% steam.

Low-angle X-ray diffraction (XRD) patterns were obtained on a Rigaku D/Max-2500/PC diffractometer (Japan) with a Cu Kα radiation ($\lambda = 0.15418$ nm) source operating at 30 kV and 40 mA. The diffraction patterns were collected from 0.6° to 2.0° at 0.02° intervals with a rate of $1(^\circ)\cdot\text{min}^{-1}$. The crystal phase was identified according to Ref. [18]. The pore sizes and surface areas of the support materials were measured by nitrogen adsorption–desorption method at liquid nitrogen temperature with a surface area and pore size analyzer (JW-BK122F, Beijing JWGB Sci. & Tech., China). Samples were degassed at 220 °C for 1 h under vacuum environment before measurements. Morphologies of Pt/KIT samples were taken using transmission electron microscope (TEM, JEOL 2100, Japan). To prepare TEM sample, ultrasonic oscillation was used to make sample uniformly disperse in ethanol, and then two droplets of solution were made on a copper grid for supporting a perforated carbon film.

The pulse CO chemisorption method (Autochem II 2920, Micromeritics Co.) was used to measure the dispersion of active Pt species. Details of the procedure for CO chemisorption were described elsewhere [19]. The dispersion and particle size of platinum were calculated by the following equations in Refs. [19, 20]

$$D_{\text{Pt}}(\%) = 100 \times \frac{V_{\text{S}}/f}{22.414 C_{\text{S}} W_{\text{S}}} \times M \tag{1}$$

$$d_{\text{Pt}} = \frac{6 \times 10^9 C_{\text{a}} M V_{\text{S}}}{\rho N_{\text{a}} D_{\text{Pt}}} \tag{2}$$

where D_{Pt} is the metal dispersion of Pt, V_{S} is the CO volume adsorbed at STP (ml), f is the stoichiometric factor which equals to 1, C_{S} is Pt metal content equals to 1 wt%, W_{S} is the weight of sample (g), M is Pt atomic mass, d_{Pt} is the particle size of Pt, C_{a} is the surface metal concentration equals to 1.25×10^{19} atoms·m^{-2}, ρ is the volume mass equals to 21.45×10^6 g·m^{-3}, and N_{a} is Avogadro constant.

For the catalytic activity test, 100 mg catalyst was mixed with 500 mg quartz sands to keep catalytic even heated during reaction. The mixture was loaded in a

reaction tube with diameter of 10 mm. The catalytic activity was evaluated by passing a gas mixture of 1000×10^{-6} C_3H_8, 2% O_2 and N_2 in balance. The space velocity was 60,000 h^{-1}. The reactor was heated from room temperature to 500 °C at a heating rate of 10 °C·min^{-1} after N_2 pretreatment at 500 °C for 30 min. The outlet gas from the reactor was analysed by Fourier transform infrared spectroscopy (FTIR) gas analyzer (MKS MultiGas 2030, USA).

3 Results and discussion

3.1 Low-angle XRD characterization

The ordered mesoporous structure can be identified by low-angle XRD. It can be found from the low-angle XRD patterns in Fig. 1 that all the three support materials perform one major characteristic diffraction peak at $2\theta = 0.98°$–$1.15°$, corresponding to (211) plane [18, 21, 22]. A series of overlapping peaks (1.5°–2.0°) appearing in KIT-6-80 and KIT-6-130 are responsible for (220) and (420) planes [21]. The appearance of such peaks suggests the typical ordered mesoporous structure three-dimensional (3D) *Ia3d* cubic space group in KIT-6 [18, 21]. The appearance of the overlapping peaks (1.5°–2.0°) in KIT-6-80 and KIT-6-130 means that they have better ordered mesoporous structure than KIT-6-40. The difference of hydrothermal treatment temperature seems not to change the main structure but affects the peak positions. The shift of main peaks to smaller 2θ suggests

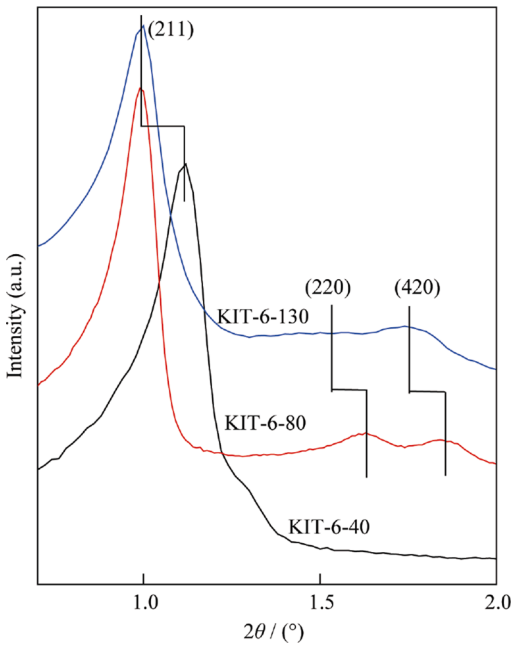

Fig. 1 Low-angle XRD patterns of KIT-6 samples

the larger scale of the porous array in KIT-6-80 and even larger in KIT-6-130. The Pt loading has no influence on the structures, so that the similar XRD patterns of the three Pt/KIT-6 catalysts are not shown in present work.

3.2 Pore structures

The N_2 adsorption–desorption isotherm curves at 77 K of the samples are shown in Fig. 2a, where p and p_0 represent the equilibrium and the saturation pressure of adsorbates at the temperature of adsorption, respectively. According to category sorted by International Union of Pure and Applied Chemistry (IUPAC) [23], the adsorption curves are typical type IV curves which confirm the mesoporous structure of the samples. KIT-6-130 gets saturated at a relatively higher pressure than KIT-6-80 and KIT-6-40, suggesting its larger average pore size. The desorption process of all the three support materials requires lower relative pressure and shows H1-type hysteresis loop in the graph. It indicates the typical capillary condensation and uniform pores over the tested KIT-6 samples. The curve of KIT-6-40 performs much lower adsorbed quantity, and the hysteresis loop shifts to the left side in comparison to those of the other two samples, which means the smaller pore size and lower surface area, respectively. The corresponding pore size distributions of the three KIT-6 samples are shown in Fig. 2b. It directly reveals that the three support samples exhibit distinct pore sizes, which follow the sequence of KIT-6-130 (9–12 nm) > KIT-6-80 (7–9 nm) > KIT-6-40 (4–6 nm). It confirms the predicted trend of the porous size in above XRD analysis. That also means that adjusting the temperature of the hydrothermal treatment during the synthesis process could effectively control the pore sizes of KIT-6.

The surface area and pore volume of the KIT-6 and Pt/KIT-6 samples are listed in Table 1. The mesoporous KIT-6 samples show large surface areas and pore volumes, with KIT-6-80 exhibiting the highest surface area of 878 $m^2 \cdot g^{-1}$, KIT-6-130 of 691 $m^2 \cdot g^{-1}$ and KIT-6-40 of 615 $m^2 \cdot g^{-1}$. The largest pore volume appears in KIT-6-130 with the pore volume of 1.678 $cm^3 \cdot g^{-1}$. Both surface area and pore volume decrease after Pt loading, which implies that the Pt species disperse not only on the surface of the KIT-6 but also in the pores.

3.3 TEM results

TEM provided a method to directly observe the ordered pore structures of KIT-6 and the size distribution of Pt particles. TEM images of the three Pt/KIT-6 samples are shown in Fig. 3. The statistical pore sizes marked on images were calculated by counting the size of 50 pores on each image. It is easily found that 3D cubic arrays of

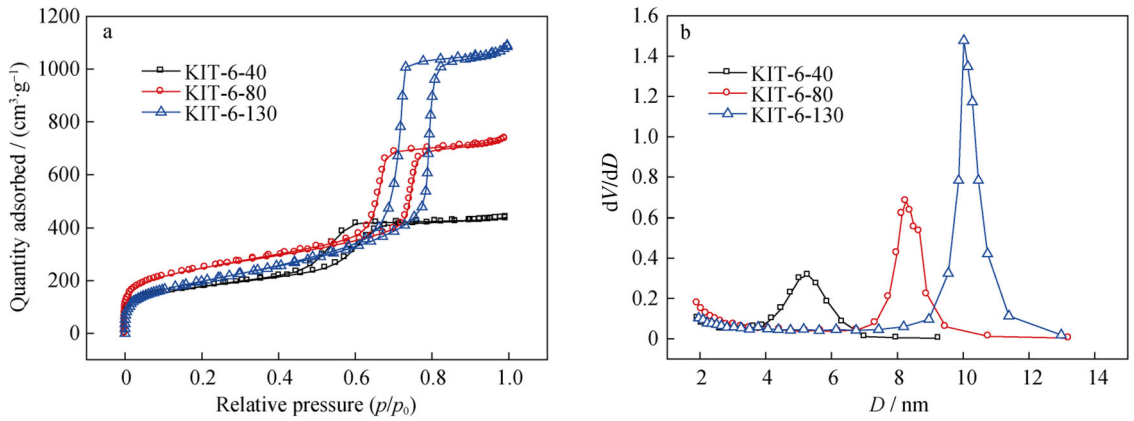

Fig. 2 N_2 adsorption/desorption isotherms **a** and pore size distribution **b** of KIT-6 samples

Table 1 Surface area (S_{BET}), pore volume, CO uptake and Pt particle sizes (d_{Pt}) of supports and Pt/supports samples

Samples	S_{BET}/($m^2 \cdot g^{-1}$)		Pore volume/($cm^3 \cdot g^{-1}$)		CO uptake/($mmol \cdot g^{-1}$)[a]	d_{Pt}/nm	
	Support	Pt/support	Support	Pt/support		CO chem.[a]	TEM[b]
KIT-6-40	615	495	0.68	0.45	23.3	2.5	–
KIT-6-80	878	783	1.14	0.88	11.3	5.1	4.3
KIT-6-130	691	597	1.68	1.44	17.8	3.5	3.7

[a] CO uptake and d_{Pt} calculated from CO chemisorption (chem.)

[b] d_{Pt} Calculated from TEM particle analysis

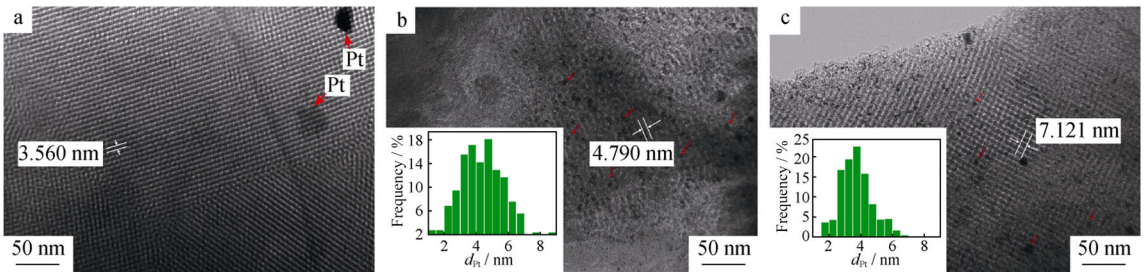

Fig. 3 TEM images of **a** Pt/KIT-6-40, **b** Pt/KIT-6-80 and **c** Pt/KIT-6-130 catalysts

mesopores in KIT-6 are conserved even after Pt loading. Most of the Pt nanoparticles (labelled by red arrows) exist in the 3D mesopores with sphere shape in Pt/KIT-6-80 (Fig. 3b) and Pt/KIT-6-130 (Fig. 3c), while few Pt particles are visible in Pt/KIT-6-40 (Fig. 3a). It reveals that both KIT-6-130 and KIT-6-80 show better Pt dispersion than Pt/KIT-6-40 (Fig. 3a). The inset figures in Fig. 3b, c display Pt size distributions determined by measuring 300 particles for Pt/KIT-6-80 and Pt/KIT-6-130, respectively. For KIT-6-130, the average pore size is measured as 7.1 nm by TEM statistic, but the observed average Pt particle size is only 3.7 nm. By contrast, KIT-6-80 shows the average pore size of $\sim$4.8 nm and the average Pt particle size of 4.3 nm. It is worthy to mention that Pt/KIT-6-80 sample has a narrower distribution of Pt particle sizes than Pt/KIT-6-130, although they have similar average Pt particle sizes. Such phenomenon suggests that the host with appropriate size mesopores could effectively control the scale of inside Pt nanoparticles, which is related to the "nano-confinement effects" on mesoporous materials as reported before [24–26]. Figure 2b shows the pore size distribution of the three samples, where D and dV/dD are the pore size and the pore volume variation with pore size, respectively. The results reveal that the average pore size of KIT-6-40 is 3.5 nm, but with few Pt particles observed in TEM images. That might be caused by the overlap of shadow and particle, or Pt could not be accommodated in the pores of KIT-6-40 because of its too small pore size.

3.4 CO chemisorption

To obtain the more statistic data on Pt dispersion, the three Pt/KIT-6 samples were characterized by CO chemisorption method. The CO uptake and the deduced particle sizes of Pt are shown in Table 1. The deduced Pt particle sizes in Pt/KIT-6-80 and Pt/KIT-6-130 are close to those measured in TEM images (Fig. 3b, c). It is found that Pt/KIT-6-40 displays very large CO uptake (23.3 $mmol \cdot g^{-1}$), indicating the successful loading of Pt species on KIT-6-40 although they are not observed in TEM image (Fig. 3a). That means the more highly dispersed Pt on the external surface of KIT-6-40. On the other hand, CO uptake on Pt/KIT-6-40 is even larger than that on Pt/KIT-6-80 or Pt/KIT-6-130 and the deduced Pt particle size in Pt/KIT-6-40 is smaller. It suggests that the more Pt species are more highly dispersed on the external surface of KIT-6-40 to benefit for direct adsorption of CO. Additionally, the small difference of Pt particle size between TEM and CO chemisorption results in Pt/KIT-6-80 and Pt/KIT-6-130 should also be contributed by those unobserved Pt species on the external surface of KIT-6-80 and KIT-6-130.

3.5 Catalytic performance

Catalytic performance of the supported Pt catalysts is reported in Fig. 4. In Fig. 4a, the Pt/KIT-6 catalysts perform good catalytic activities. The propane conversion of all the three samples rises rapidly below 200 °C. The T_{50} of the catalysts follows the sequence of Pt/KIT-6-80 (237 °C) < Pt/KIT-6-130 (248 °C) < Pt/KIT-6-40 (268 °C), which are much lower than that of the conventional Pt/Al_2O_3 catalyst in the previous literature [27]. Considering the practical serving environment of the automotive catalysts, the enforced ageing in steam/air was further carried out on such catalysts. The catalytic performance of Pt/KIT-6 samples after ageing at 800 °C with 10% saturated steam for 12 h is shown in Fig. 4b. The three aged catalysts remain satisfying catalytic performance. The T_{50} of the three samples rises by only 20–30 °C compared to that of the fresh ones, and the sequence is as aged Pt/KIT-6-80 (261 °C) < aged Pt/KIT-6-130 (276 °C) < aged Pt/KIT-6-40 (286 °C). The aged Pt/KIT-6-80 exhibits the best catalytic performance. Its HC conversion reaches upon 80% before 300 °C. However, the HC conversion of both aged Pt/KIT-6-130 and aged Pt/KIT-6-40 meets an obvious "bottleneck region" at 300–400 °C and makes a breakthrough until the temperature rises up to 450 °C.

Particle sizes and valence of Pt are the important factors of propane catalytic oxidation [28]. N_2 pretreatment at 500 °C before activity test can exclude the influence of the oxidative states of Pt on activities, so that the different catalytic performances should be mainly attributed to the particles. Researches [29, 30] showed that too fragmentary Pt particles were barriers for propane oxidation and relatively bigger Pt nanoparticles provided more active sites for breaking C–C bonding. Based on this point of view, the relatively better activity of Pt/KIT-6-80 probably benefits from the larger average Pt particle size as well as its narrow distribution. On the other hand, the mesopores on support materials effectively prevent the growing of inside Pt nanoparticles during calcining [24–26]. This would be the main reason to explain the satisfying thermal resistance of Pt/KIT-6-80 and Pt/KIT-6-130. Pt/KIT-6-40 performs not very well after ageing because of its initial highly dispersed Pt on the external surface of KIT-6-40 which could be easily sintered during thermal ageing.

4 Conclusion

Three mesoporous silica KIT-6 with different pore sizes were successful synthesized, and good catalytic performance was performed with Pt loading on propane total oxidation. Among the three catalysts, Pt/KIT-6-80 with

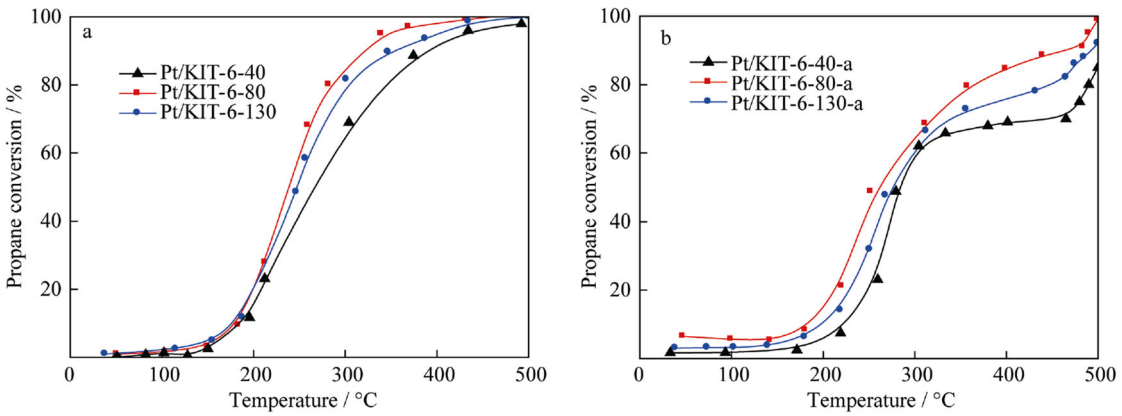

Fig. 4 C_3H_8 light-off curves of Pt/KIT-6 catalysts: **a** as-received samples and **b** hydrothermal aged samples

both appropriate pore size and Pt particle size exhibits the best catalytic performance. The mesopores on KIT-6 could effectively confine the size of the inside Pt nanoparticles during calcining. Relatively bigger Pt nanoparticles seem to be more beneficial for propane total oxidation. However, Pt particles prefer dispersing on external surface of KIT-6-40 but not in those pores with too small size.

Acknowledgements This work was financially supported by the National Key Research and Development Program of China (No. 2016YFC0205000) and the Ministry of Science and Technology of China (No. 2015AA034603).

References

[1] Cui Y, Peng H, Deng K, Shi L. The effects of unburned hydrocarbon recirculation on ignition and combustion during diesel engine cold starts. Energy. 2014;64:323.
[2] Theis JR, Lambert CK. An assessment of low temperature NO_x adsorbers for cold-start NO_x control on diesel engines. Catal Today. 2015;258(S2):367.
[3] Benard S, Ousmane M, Retailleau L, Boreave A, Vernoux P, Giroir-Fendler A. Treatment of air polluted with methanol vapours in biofilters with and without percolation. Can J Civ Eng. 2009;36(12):1935.
[4] Haneda M, Sasaki M, Hamada H, Ozawa M. In situ FT-IR study of diesel hydrocarbon oxidation over Pt/Al_2O_3 catalyst. Catal Lett. 2011;141(9):1262.
[5] Haneda M, Sasaki M, Hamada H, Ozawa M. Effect of Pt dispersion on the catalytic activity of supported Pt catalysts for diesel hydrocarbon oxidation. Top Catal. 2013;56(1–8):249.
[6] Galisteo FC, Mariscal R, Granados ML, Fierro J, Daley R, Anderson J. Reactivation of sintered Pt/Al_2O_3 oxidation catalysts. Appl Catal B. 2005;59(3):227.
[7] Yoshida H, Yazawa Y, Hattori T. Effects of support and additive on oxidation state and activity of Pt catalyst in propane combustion. Catal Today. 2003;87(1–4):19.
[8] Cao Y, Ran R, Chen Y, Wu X, Weng D. Nanostructured platinum in ordered mesoporous silica as novel efficient catalyst for propane total oxidation. RSC Adv. 2016;6(36):30170.
[9] Avila M, Vignatti C, Apesteguía C, Garetto T. Effect of support on the deep oxidation of propane and propylene on Pt-based catalysts. Chem Eng J. 2014;241:52.
[10] Iwamoto M, Yahiro H, Shin HK, Watanabe M, Guo J, Konno M, Chikahisa T, Murayama T. Performance and durability of zeolite catalyst for selective reduction of nitrogen monoxide in actual diesel-engine exhaust. Appl Catal B. 1994;5(1):L1–16.
[11] Matsubayashi N, Yasuda H, Imamura M, Yoshimura Y. Catalyst design and development for upgrading aromatic hydrocarbons. Catal Today. 1998;45(1–4):375.
[12] Lee S-W, Ihm S-K. Hydroisomerization and hydrocracking over platinum loaded ZSM-23 catalysts in the presence of sulfur and nitrogen compounds for the dewaxing of diesel fuel. Fuel. 2014; 134:237.
[13] Garetto T, Rincón E, Apesteguia C. The origin of the enhanced activity of Pt/zeolites for combustion of C-2–C-4 alkanes. Appl Catal B. 2007;73(1):65.
[14] Boulaoued A, Fechete I, Donnio B, Bernard M, Turek P, Garin F. Mo/KIT-6, Fe/KIT-6 and Mo-Fe/KIT-6 as new types of heterogeneous catalysts for the conversion of MCP. Microporous Mesoporous Mater. 2012;155:131.
[15] Liu H, Wang H, Shen J, Sun Y, Liu Z. Preparation, characterization and activities of the nano-sized Ni/SBA-15 catalyst for producing CO_x-free hydrogen from ammonia. Appl Catal A. 2008;337(2):138.
[16] Anpo M, Yamashita H, Ikeue K, Fujii Y, Zhang SG, Ichihashi Y, Park DR, Suzuki Y, Koyano K, Tatsumi T. Photocatalytic reduction of CO_2 with H_2O on Ti-MCM-41 and Ti-MCM-48 mesoporous zeolite catalysts. Catal Today. 1998;44(1):327.
[17] Soni K, Rana BS, Sinha AK, Bhaumik A, Nandi M, Kumar M, Dhar GM. 3-D ordered mesoporous KIT-6 support for effective hydrodesulfurization catalysts. Appl Catal B. 2009;90(1–2):55.
[18] Kleitz F, Hei Choi S, Ryoo R. Cubic Ia3d large mesoporous silica: synthesis and replication to platinum nanowires, carbon nanorods and carbon nanotubes. Chem Commun. 2003;17:2136.
[19] Cao Y, Ran R, Wu X, Weng D. A new insight into the effects of barium addition on Pd-only catalysts: Pd-support interface and CO + NO reaction pathway. Appl Catal A. 2015;501:17.
[20] Bowker M, Stone P, Morrall P, Smith R, Bennett R, Perkins N, Kvon R, Pang C, Fourre E, Hall M. Model catalyst studies of the strong metal-support interaction: surface structure identified by STM on Pd nanoparticles on TiO_2(110). J Catal. 2005;234(1): 172–81.
[21] Patel A, Shukla P, Rufford T, Wang S, Chen J, Rudolph V, Zhu Z. Catalytic reduction of NO by CO over copper-oxide supported mesoporous silica. Appl Catal A. 2011;409:55.
[22] Zhang D, Duan A, Zhao Z, Xu C. Synthesis, characterization, and catalytic performance of NiMo catalysts supported on hierarchically porous Beta-KIT-6 material in the hydrodesulfurization of dibenzothiophene. J Catal. 2010;274(2):273.
[23] Sing KS, Evrett DH, Haul RAW, Moscou L, Pierotti RA, Rouqerol J, Siemieniewska T. Reporting physisorption data for gas/solid systems with special reference to the determination of surface area and porosity. Pure Appl Chem. 1985;57(4):603.
[24] Rafti M, Brunsen A, Fuertes MC, Azzaroni O, Soler-Illia GJ. Heterogeneous catalytic activity of platinum nanoparticles hosted in mesoporous silica thin films modified with polyelectrolyte brushes. ACS Appl Mater Interfaces. 2013;5(18):8833.
[25] Huang S, Hara K, Fukuoka A. Green catalysis for selective CO oxidation in hydrogen for fuel cell. Energy Environ Sci. 2009; 2(10):1060.
[26] Díaz U, Brunel D, Corma A. Catalysis using multifunctional organosiliceous hybrid materials. Chem Soc Rev. 2013;42(9): 4083.
[27] Garetto T, Rincón E, Apesteguıa C. Deep oxidation of propane on Pt-supported catalysts: drastic turnover rate enhancement using zeolite supports. Appl Catal B. 2004;48(3):167.
[28] Park JE, Kim KB, Kim Y-A, Song KS, Park ED. Effect of Pt particle size on propane combustion over Pt/ZSM-5. Catal Lett. 2013;143(11):1132.
[29] Beck IE, Bukhtiyarov VI, Pakharukov IY, Zaikovsky VI, Kriventsov VV, Parmon VN. Platinum nanoparticles on Al_2O_3: correlation between the particle size and activity in total methane oxidation. J Catal. 2009;268(1):60.
[30] Otto K, Andino JM, Parks C. The influence of platinum concentration and particle size on the kinetics of propane oxidation over Pt/γ-alumina. J Catal. 1991;131(1):243.